PERGAMON

International Journal of Solids and Structures 39 (2002) 2257–2279

INTERNATIONAL JOURNAL OF SOLIDS and STRUCTURES

www.elsevier.com/locate/ijsolstr

Low-energy impact of adaptive cylindrical piezoelectric–composite shells

Dimitris A. Saravanos [a,*], Andreas P. Christoforou [b]

[a] *Department of Mechanical Engineering and Aeronautics, University of Patras, Patras, GR 26500, Greece*
[b] *Department of Mechanical Engineering, Kuwait University, 13060 Kuwait*

Received 19 March 2001; received in revised form 26 December 2001

Abstract

A theoretical framework for analyzing low-energy impacts of laminated shells with active and sensory piezoelectric layers is presented, including impactor dynamics and contact law. The formulation encompasses a coupled piezoelectric shell theory mixing first order shear displacement assumptions and layerwise variation of electric potential. An exact in-plane Ritz solution for the impact of open cylindrical piezoelectric–composite shells is developed and solved numerically using an explicit time integration scheme. The active impact control problem of adaptive cylindrical shells with distributed curved piezoelectric actuators is addressed. The cases of optimized state feedback controllers and output feedback controllers using piezoelectric sensors are analyzed. Numerical results quantify the impact response of cylindrical shells of various curvatures including the signal of curved piezoelectric sensors. Additional numerical studies quantify the impact response of adaptive cylindrical panels and investigate the feasibility of actively reducing the impact force.

Keywords: Composites; Laminates; Piezoelectrics; Shells; Impact; Adaptive structures; Smart materials; Sensors; Actuators; Controller

1. Introduction

Smart structures that can sense and adapt to changes in their loads and environment are highly desirable since they provide, among other things, new opportunities and flexibility in designing damage tolerant and stable structures. Such opportunities exist in the critical area of developing impact tolerant composite structures. Foreign object impacts are common threats to many structural applications, increasing the safety risk and reducing the effectiveness and reliability of composite structures as primary loading members. Impacts are complex events, and depending on the impactor/structure characteristics and interactions, the resulting damage may be either visible or hidden. Therefore, adaptive piezoelectric laminates with embedded piezoelectric sensors and actuators may be good candidates for monitoring or even shaping the impact event, leading to better damage resistance, impact parameter identification and damage

* Corresponding author. Fax: +30-61-997-234.
E-mail address: saravanos@mech.upatras.gr (D.A. Saravanos).

0020-7683/02/$ - see front matter
PII: S0020-7683(02)00087-2

assessment. This paper addresses the development of an analytical method for quantifying the response of adaptive piezoelectric–composite shells in low-energy impacts.

In general, the impact of composite structures has received a lot of attention in recent years. Analytical, computational, experimental and combined studies have utilized simple structures, such as beams, plate and shells to investigate impact response and damage. Beams and plates have received most of the attention (see e.g., Sankar and Sun (1985), Cairns and Lagace (1989), Qian and Swanson (1990), Christoforou and Swanson (1991), Prasad et al. (1994), Yigit and Christoforou (1995), Pierson and Vaziri (1996) and Christoforou and Yigit (1998a)), while less effort seems to have been directed towards shells, mainly because of the added complexity in the field equations (see e.g., Christoforou and Swanson (1990), Swanson et al. (1991), Vaziri et al. (1996) and Matemilola and Stronge (1997)). On the other hand, substantial effort has been directed towards the mechanics of piezoelectric–composite laminates and structures and the study of their dynamic response (see e.g., the reviews by Sunar and Rao (1999) and Saravanos and Heyliger (1999)), as well as, the active vibration and shape control with adaptive piezoelectric structures (see e.g., Baz and Poh (1988), Tzou and Tseng (1990), Chantrashekhara and Agarwal (1993), Kokonis et al. (1994), Abramovich (1998), Ray (1998) and Liu et al. (1999)).

Yet, the impact of smart structures has received minimal attention. Work has been reported mainly in impact load identification by Choi and Chang (1996) and Tracy and Chang (1998), in the reduction of impact stresses using shape memory alloys by Birman et al. (1997), in active control of blast-loaded piezoelectric beams by Librescu and Na (1998), and in the impact control of plates using concentrated force actuators by Yigit and Christoforou (2000). Saravanos and Christoforou (2000) investigated the impact response of adaptive piezoelectric laminated plates using an exact Ritz model with a coupled piezoelectric laminate theory. Among other things, it was demonstrated that for moderate to heavy mass impacts, the use of optimized linear quadratic regulator (LQR) or sensory feedback controllers could reduce the impact force.

As mentioned previously, piezoelectric–composite laminates may be good candidates for detecting and monitoring the impact event in composite shell structures. Effective achievement of this task requires piezoelectric laminate mechanics that can accurately model the full electromechanical response of the shell, as well as, provide insight into the impact event. This paper extends the previous work to composite shells with *distributed* piezoelectric sensors and actuators. While the basic approach is seemingly similar, the development of mechanics and models for analyzing the impact of adaptive piezoelectric shells involves additional challenges, because of the more involved mechanics and the extension–bending coupling effects induced by the shell curvature on the overall characteristics of the impact event. The presence of curved piezoelectric sensors and actuators in impacted shell structures also requires special consideration. The present paper describes mechanics and a Ritz solution for analyzing low-energy impacts on cylindrical piezocomposite shells with distributed actuators and sensors. Attention is mainly focused on the global response of the impacted shell, the direct inclusion of impactor-target dynamic interactions, and the implementation of a realistic contact law into the model. The work addresses "low-energy" impacts and does not consider other non-linear phenomena, such as, damage initiation and propagation into the piezoelectric laminate. However, the present mechanics establishes the theoretical framework for addressing such complex issues in future studies. The model of the adaptive shell is subsequently formulated by integrating the shell-impactor system with optimal state feedback or output feedback controllers for the active control of critical impact parameters.

2. Piezoelectric shell laminate

This section briefly describes the new elements of the theoretical framework required for analyzing the target dynamics, that is, the coupled dynamic behavior of a shell laminate with embedded piezoelectric actuators and sensors.

2.1. Material equations

The impact target, a curvilinear laminate consisting of composite plies and embedded piezoelectric layers, is shown schematically in Fig. 1. Each ply of the laminate remains parallel to a reference curvilinear surface A_0. An orthogonal curvilinear coordinate system $\bar{O}\xi\eta\zeta$ is defined, such that the axes ξ and η lie on the curvilinear reference surface A_0, while axis ζ remains straight and perpendicular to the layers of the laminate. Each ply is generally assumed to consist of a linear piezoelectric material with properties defined on the orthogonal curvilinear system $\bar{O}\xi\eta\zeta$, and constitutive equations of the following form,

$$\begin{aligned} \overline{\sigma}_i &= C_{ij}^{\mathrm{E}}\overline{S}_j - e_{ik}\overline{E}_k \\ \overline{D}_l &= e_{lj}\overline{S}_j + \varepsilon_{lk}^{\mathrm{S}}\overline{E}_k \end{aligned} \tag{1}$$

where $i, j = 1, \ldots, 6$ and $k, l = 1, \ldots, 3$; σ_i and S_i are the mechanical stresses and engineering strains in vectorial notation; E_k, the electric field vector; D_l, the electric displacement vector; C_{ij}, the elastic stiffness tensor; e_{lj}, the piezoelectric tensor; and ε_{lk}, the electric permittivity tensor of the material. The overbar indicates quantities expressed in the curvilinear system, while superscripts E, and S indicate constant electric field and strain conditions, respectively. The axes 1, 2, and 3 of the material are parallel to the curvilinear axes ξ, η, and ζ, respectively. The materials are assumed to be monoclinic class 2 crystals with a polarization axis parallel to the ζ axis.

Dropping the overbar in the remaining paper, the strain–displacement relationships are (Soedel, 1993; Saravanos, 1997),

$$\begin{aligned} S_{11} = S_1 &= \frac{1}{g_{11}}\left(u_{,\xi} + \frac{g_{11,\eta}^0}{g_{22}^0}v + \frac{g_{11}^0}{R_1}w\right) \\ S_{22} = S_2 &= \frac{1}{g_{22}}\left(v_{,\eta} + \frac{g_{22,\xi}^0}{g_{11}^0}u + \frac{g_{22}^0}{R_2}w\right) \\ S_{12} = S_6 &= \frac{1}{g_{11}}\left(v_{,\xi} - \frac{g_{11,n}^0}{g_{22}^0}u\right) + \frac{1}{g_{22}}\left(u_{,\eta} - \frac{g_{22,\xi}^0}{g_{11}^0}v\right) \\ S_{33} = S_3 &= w_{,\zeta} \\ S_{23} = S_4 &= v_{,\zeta} + \frac{1}{g_{22}}\left(w_{,\eta} - \frac{g_{22}^0}{R_2}v\right) \\ S_{13} = S_5 &= u_{,\zeta} + \frac{1}{g_{11}}\left(w_{,\xi} - \frac{g_{11}^0}{R_1}u\right) \end{aligned} \tag{2}$$

where u, v, w are displacements in the curvilinear system. The relation of electric field vector E_k to the electric potential φ is (Tzou and Zhong, 1993; Saravanos, 1997),

$$\begin{aligned} E_1 &= -\frac{1}{g_{11}}\varphi_{,\xi} \\ E_2 &= -\frac{1}{g_{22}}\varphi_{,\eta} \\ E_3 &= -\varphi_{,\zeta} \end{aligned} \tag{3}$$

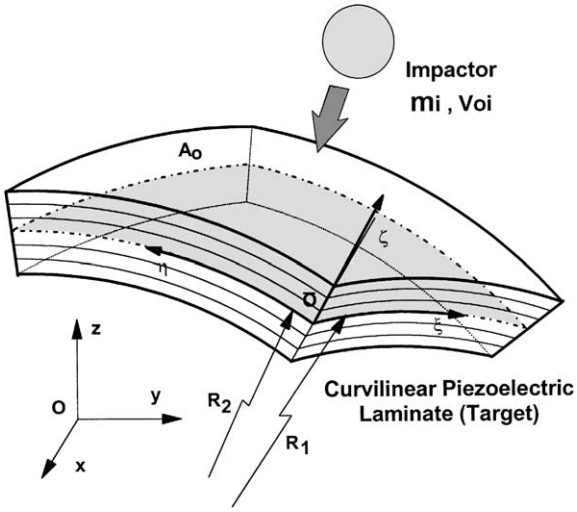

Fig. 1. Impacted curvilinear piezoelectric laminate and coordinate systems.

where, the components of the metric tensor are defined as,

$$g_{11} = (1 + \zeta/R_1)g^0_{11}, \quad g_{22} = (1 + \zeta/R_2)g^0_{22} \tag{4}$$

R_i are the local radii of curvature, and g^0_{11}, g^0_{22} are the metric tensor components on the surface A_0 ($\zeta = 0$), respectively. It is proved that the equilibrium equations are for the stresses,

$$\begin{aligned}
&(g_{22}\sigma_{11})_{,\xi} + (g_{11}\sigma_{12})_{,\eta} + (g_{11}g_{22}\sigma_{13})_{,\zeta} - g_{11}\frac{g^0_{22,\xi}}{g^0_{11}}\sigma_{22} + g_{22}\frac{g^0_{11,\eta}}{g^0_{22}}\sigma_{12} + g_{22}\frac{g^0_{11}}{R_1}\sigma_{13} - g_{11}g_{22}\rho\ddot{u} = 0\\
&(g_{22}\sigma_{12})_{,\xi} + (g_{11}\sigma_{22})_{,\eta} + (g_{11}g_{22}\sigma_{23})_{,\zeta} + g_{11}\frac{g^0_{22,\xi}}{g^0_{11}}\sigma_{12} - g_{22}\frac{g^0_{11,\eta}}{g^0_{22}}\sigma_{11} + g_{11}\frac{g^0_{22}}{R_2}\sigma_{23} - g_{11}g_{22}\rho\ddot{v} = 0\\
&(g_{22}\sigma_{13})_{,\xi} + (g_{11}\sigma_{23})_{,\eta} + (g_{11}g_{22}\sigma_{33})_{,\zeta} - g_{22}\frac{g^0_{11}}{R_1}\sigma_{11} - g_{11}\frac{g^0_{22}}{R_2}\sigma_{22} - g_{11}g_{22}\rho\ddot{w} = 0
\end{aligned} \tag{5}$$

and for the electric displacements,

$$(g_{22}D_1)_{,\xi} + (g_{11}D_2)_{,\eta} + (g_{11}g_{22}D_3)_{,\zeta} = 0 \tag{6}$$

2.2. Laminate shell theory

The coupled piezoelectric shell theory (Saravanos, 1997) is applied to yield the generalized laminate governing equations. The theory assumes linear displacement fields through the thickness of the laminate, together with a layerwise electric potential field consisting of N discrete continuous segments. The displacements and electric potential of the mixed-field theory take the following form,

$$
\begin{aligned}
u(\xi,\eta,\zeta,t) &= u^0(\xi,\eta,t) + \zeta\beta_\xi(\xi,\eta,t)\\
v(\xi,\eta,\zeta,t) &= v^0(\xi,\eta,t) + \zeta\beta_\eta(\xi,\eta,t)\\
w(\xi,\eta,\zeta,t) &= w^0(\xi,\eta,t)\\
\varphi(\xi,\eta,\zeta,t) &= \sum_{j=1}^{N}\varphi^j(\xi,\eta,t)\Psi^j(\zeta)
\end{aligned}
\tag{7}
$$

where u^0, v^0, w^0 are the displacements on the reference surface A_0, along the ξ, η and ζ axes; superscript j indicates the points ζ^j at the interface of each discrete layer; φ^j is the electric potential at each point ζ^j; $\Psi^j(\zeta)$ are interpolation functions; and β_ξ, β_η are the flexural rotation angles.

Shallow shells are further assumed $(1+\zeta/R_i \cong 1)$. Now, in the context of Eqs. (2) and (7), the engineering strains at a point of the laminate, become

$$
\begin{aligned}
S_i(\xi,\eta,\zeta,t) &= S_i^0(\xi,\eta,t) + \zeta k_i(\xi,\eta,t), \quad i=1,2,6\\
S_3(\xi,\eta,\zeta,t) &= 0\\
S_i(\xi,\eta,\zeta,t) &= S_i^0(\xi,\eta,t), \quad i=4,5
\end{aligned}
\tag{8}
$$

where S^0 and k are the mid-strain and curvature vectors at the reference surface, defined in Appendix A. The electric field vector, Eq. (3), also becomes,

$$
\begin{aligned}
E_i(\xi,\eta,\zeta,t) &= \sum_{j=1}^{N} E_i^j(\xi,\eta,t)\Psi^j(\zeta), \quad i=1,2\\
E_3(\xi,\eta,\zeta,t) &= \sum_{j=1}^{N} E_3^j(\xi,\eta,t)\Psi^j_{,\zeta}(\zeta)
\end{aligned}
\tag{9}
$$

where E^j is the generalized electric field vector defined as:

$$
E_1^j = -\frac{\Phi^j_{,\xi}}{g_{11}^0}, \quad E_2^j = -\frac{\Phi^j_{,\eta}}{g_{22}^0}, \quad E_3^j = -\Phi^j \tag{10}
$$

2.3. Laminate dynamics

It is now possible to obtain $5+N$ laminate equations of motion, by integrating Eqs. (5) and (6) through the thickness of the laminate, describing the equilibrium of forces,

$$
\begin{aligned}
&\frac{N_{1,\xi}}{g_{11}^0} + \frac{N_{6,\eta}}{g_{22}^0} + \frac{g_{22,\xi}^0}{g_{11}^0 g_{22}^0}(N_1 - N_2) + 2\frac{g_{11,\eta}^0}{g_{11}^0 g_{22}^0}N_6 + \frac{N_5}{R_1} - (\rho^A\ddot{\boldsymbol{u}}^0 + \rho^B\ddot{\boldsymbol{\beta}}_\xi^0) = -g_{11}^0 g_{22}^0 q_5\\
&\frac{N_{6,\xi}}{g_{11}^0} + \frac{N_{2,\eta}}{g_{22}^0} + \frac{g_{11,n}^0}{g_{11}^0 g_{22}^0}(N_2 - N_1) + 2\frac{g_{22,\xi}^0}{g_{11}^0 g_{22}^0}N_6 + \frac{N_4}{R_2} - (\rho^A\ddot{\boldsymbol{v}}^0 + \rho^B\ddot{\boldsymbol{\beta}}_\eta^0) = -g_{11}^0 g_{22}^0 q_4\\
&\frac{N_{5,\xi}}{g_{11}^0} + \frac{N_{4,\eta}}{g_{22}^0} + \frac{1}{g_{11}^0 g_{22}^0}(g_{22,\xi}N_5 + g_{11,\eta}^0 N_4) - \frac{N_1}{R_1} - \frac{N_2}{R_2} - \rho^A\ddot{\boldsymbol{w}}^0 = -g_{11}^0 g_{22}^0 q_3
\end{aligned}
\tag{11}
$$

equilibrium of moments,

$$\begin{aligned}
&\frac{M_{1,\xi}}{g_{11}^0}+\frac{M_{6,\eta}}{g_{22}^0}+\frac{g_{22,\xi}^0}{g_{11}^0 g_{22}^0}(M_1-M_2)+\frac{2g_{11,\eta}^0}{g_{11}^0 g_{22}^0}M_6+\frac{M_5}{R_1}-N_5-(\rho^B\ddot{u}^0+\rho^D\beta_{\ddot{\xi}}^0)=0\\
&\frac{M_{6,\xi}}{g_{11}^0}+\frac{M_{2,\eta}}{g_{22}^0}+\frac{g_{11,\eta}^0}{g_{11}^0 g_{22}^0}(M_2-M_1)+\frac{2g_{22,\xi}^0}{g_{11}^0 g_{22}^0}M_6+\frac{M_4}{R_2}-N_4-(\rho^B\ddot{v}^0+\rho^D\beta_{\ddot{\eta}}^0)=0
\end{aligned} \tag{12}$$

and conservation of generalized electric charges,

$$\frac{D_{1,\xi}^m}{g_{11}^0}+\frac{D_{2,\eta}^m}{g_{22}^0}-D_3^m+\frac{1}{g_{11}^0 g_{22}^0}(g_{22,\xi}^0 D_1^m+g_{11,\eta}^0 D_2^m)=-g_{11}^0 g_{22}^0\overline{D}_3^m,\quad m=1,\ldots,N \tag{13}$$

where, ρ^A, ρ^B, and ρ^D are generalized densities defined in Appendix A and express the mass, mass coupling and rotational inertia of the laminate, respectively; q_3, q_4, q_5 are respectively the normal and shear surface tractions. The resultant forces N_i, moments M_i, and electric displacements D_i^m in the previous equations are defined as follows:

$$\langle N_i, M_i\rangle = g_{11}^0 g_{22}^0\int_0^h \sigma_i\langle 1,\zeta\rangle\,\mathrm{d}\zeta,\quad i=1,2,4,5,6 \tag{14}$$

$$\begin{aligned}
&\langle D_1^m, D_2^m\rangle = g_{11}^0 g_{22}^0\int_0^h \langle D_1, D_2\rangle\Psi^m(\zeta)\,\mathrm{d}\zeta\\
&D_3^m = g_{11}^0 g_{22}^0\int_0^h D_3\Psi_{,\zeta}^m(\zeta)\,\mathrm{d}\zeta,\quad m=1,\ldots,N
\end{aligned} \tag{15}$$

The resultant generalized constitutive relations between generalized stress and electric displacement, and generalized strain and electric field are shown in Appendix A.

3. Cylindrical piezoelectric shells under impact

The formulation of the governing equations in the orthogonal curvilinear system and the attained separation of the through-the-thickness integration in the equations of motion (11)–(13) enables the development of exact structural solutions on the reference surface A_0 for select geometries, laminations and boundary conditions. Such a solution is described herein for simply supported cylindrical shells with distributed piezoelectric (piezopolymer or piezoceramic) actuators and sensors. It is assumed that all piezoelectric layers and composite plies are orthotropic ($C_{16}=C_{26}=e_{36}=0$); and the axis η remains parallel to the axis of revolution of the cylindrical shell, while axes ξ and ζ represent the hoop and radial directions respectively, then $1/R_2=g_{11,\eta}^0=g_{22,\xi}^0=0$, $g_{22}^0=1$, and R_1, g_{11}^0 remain constant over A_0.

3.1. Shell dynamics

For a cylindrical piezoelectric laminate, Eqs. (11) and (12) are simplified and yield the following five differential equations after their combination with the laminate constitutive equations:

$$
\begin{aligned}
&\frac{1}{g_{11}^0}\left(A_{11}S_{1,\xi}^0+A_{12}S_{2,\xi}^0+B_{11}k_{1,\xi}+B_{12}k_{2,\xi}-\sum_{m=1}^{N}\overline{E}_{31}^m E_{3,\xi}^m\right)+\left(A_{66}S_{6,\eta}^0+B_{66}k_{6,\eta}\right)\\
&\quad+\frac{1}{R_1}\left(A_{55}S_5^0-\sum_{m=1}^{N}\overline{E}_{15}^m E_1^m\right)-\left(\rho^A\ddot{u}^0+\rho^B\ddot{\beta}_\xi^0\right)=-g_{11}^0 q_5\\
&\frac{1}{g_{11}^0}\left(A_{66}S_{6,\xi}^0+B_{66}k_{6,\xi}\right)+\left(A_{21}S_{1,\eta}^0+A_{22}S_{2,\eta}^0+B_{21}k_{1,\eta}+B_{22}k_{2,\eta}-\sum_{m=1}^{N}\overline{E}_{32}^m E_{3,\eta}^m\right)\\
&\quad-\left(\rho^A\ddot{v}^0+\rho^B\ddot{\beta}_\eta^0\right)=-g_{11}^0 q_4\\
&\frac{1}{g_{11}^0}\left(A_{55}S_{5,\xi}^0-\sum_{m=1}^{N}\overline{E}_{15}^m E_{1,\xi}^m\right)+\left(A_{44}S_{4,\eta}^0-\sum_{m=1}^{N}\overline{E}_{24}^m E_{2,\eta}^m\right)\\
&\quad-\frac{1}{R_1}\left(A_{11}S_1^0+A_{12}S_2^0+B_{11}k_1+B_{12}k_2-\sum_{m=1}^{N}\overline{E}_{31}^m E_3^m\right)-\rho^A\ddot{w}^0=-g_{11}^0 q_3\\
&\frac{1}{g_{11}^0}\left(B_{11}S_{1,\xi}^0+B_{12}S_{2,\xi}^0+D_{11}k_{1,\xi}+D_{12}k_{2,\xi}-\sum_{m=1}^{N}\hat{E}_{31}^m E_{3,\xi}^m\right)+\left(B_{66}S_{6,\eta}^0+D_{66}k_{6,\eta}\right)\\
&\quad-\left(A_{55}S_5^0-\sum_{m=1}^{N}\overline{E}_{15}^m E_1^m\right)-\left(\rho^B\ddot{u}^0+\rho^D\ddot{\beta}_\xi^0\right)=0\\
&\frac{1}{g_{11}^0}\left(B_{66}S_{6,\xi}^0+D_{66}k_{6,\xi}\right)+\left(B_{21}S_{1,\eta}^0+B_{22}S_{2,\eta}^0+D_{21}k_{1,\eta}+D_{22}k_{2,\eta}-\sum_{m=1}^{N}\hat{E}_{32}^m E_{3,\eta}^m\right)\\
&\quad-\left(A_{44}S_4^0-\sum_{m=1}^{N}\bar{E}_{24}^m E_2^m\right)-\left(\rho^B\ddot{v}^0+\rho^D\ddot{\beta}_\eta^0\right)=0
\end{aligned}
\tag{16}
$$

Similarly, the N charge conservation equations, Eq. (13), yield the following N differential equations,

$$
\begin{aligned}
&\frac{1}{g_{11}^0}\left(\overline{E}_{15}^n S_{5,\xi}^0+\sum_{m=1}^{N}G_{11}^{nm}E_{1,\xi}^m\right)+\left(\overline{E}_{24}^n S_{4,\eta}^0+\sum_{m=1}^{N}G_{22}^m E_{2,\eta}^m\right)-\left(\overline{E}_{31}^n S_1^0+\overline{E}_{32}^n S_2^0+\hat{E}_{31}^n k_1+\hat{E}_{32}^n k_2+\sum_{m=1}^{N}G_{33}^{nm}E_3^m\right)\\
&\quad=-g_{11}^0 Q_3^n,\quad n=1,\ldots,N
\end{aligned}
\tag{17}
$$

Incorporating Eqs. (A.1) and (A.2) into Eqs. (16) and (17), a coupled system of $N+5$ differential equations with five unknown displacements $\{u^0, v^0, w^0, \beta_\xi, \beta_\eta\}$ and N unknown electric potentials $\{\phi^1,\ldots,\phi^N\}$ results. Fundamental sets of modal solutions which exactly satisfy the coupled equations may be found for at least one type of shells of practical interest, that is, simply supported open cylindrical panels (see Fig. 2a). The boundary conditions are $v^0(\xi,0)=v^0(\xi,L_\eta)=u^0(0,\eta)=u^0(L_\xi,\eta)=w^0(\xi,0)=w^0(\xi,L_\eta)=w^0(0,\eta)=w^0(L_\xi,\eta)=0$ and $\Phi^j(\xi,0)=\Phi^j(\xi,L_\eta)=\Phi^j(0,\eta)=\Phi^j(L_\xi,\eta)=0$, and the fundamental set of solutions satisfying exactly Eqs. (16) and (17) is,

$$
\begin{aligned}
&u^0(\xi,\eta,t)=U_{kl}^0(t)\cos(a\xi)\sin(b\eta),\quad v^0(\xi,\eta,t)=V_{kl}^0(t)\sin(a\xi)\cos(b\eta)\\
&w^0(\xi,\eta,t)=W_{kl}^0(t)\sin(a\xi)\sin(b\eta)\\
&\beta_\xi(\xi,\eta,t)=B_{\xi kl}(t)\cos(a\xi)\sin(b\eta),\quad \beta_\eta(\xi,\eta,t)=B_{\eta kl}(t)\sin(a\xi)\cos(b\eta)\\
&\varphi^j(\xi,\eta,t)=\Phi_{kl}^j(t)\sin(a\xi)\sin(b\eta),\quad a=k\pi/L_\xi,\ \ b=l\pi/L_\eta,\ \ k,l=1,2,3,\ldots
\end{aligned}
\tag{18}
$$

where, subscripts $k, l = 1, 2, 3, \ldots$ indicate the mode order along ξ and η axes respectively, and imply summation of the mode in the total transient response of the shell; U_{kl}^0, V_{kl}^0 W_{kl}^0, $B_{\xi kl}$, $B_{\eta kl}$, Φ_{kl}^j represent the participation factors (or gains) of the respective mode in the total response of the shell; L_ξ, L_η are the dimensions of the panel along the cylindrical coordinate axes. Substituting the previous modal solutions into

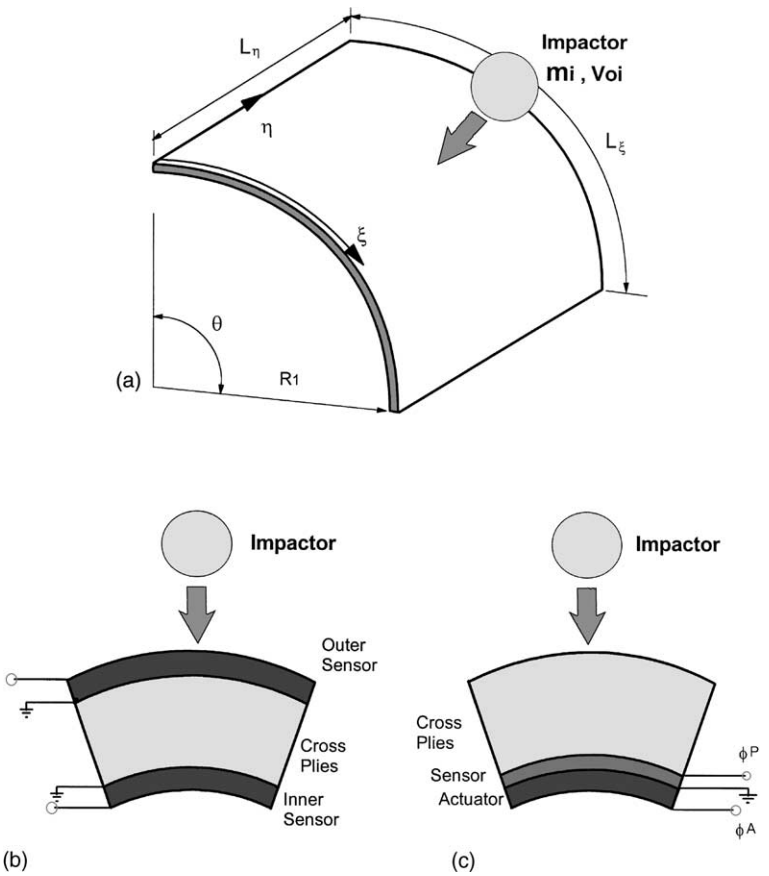

Fig. 2. Cylindrical piezoelectric shells. (a) Simply supported open cylindrical panel impacted at convex side; (b) $[p^{\mathrm{P}}/(0/90)_2/0]_{\mathrm{s}}$ laminate with two sensory layers; (c) $[(0/90)_2/0_2/(90/0)_2/p^{\mathrm{P}}/p^{\mathrm{A}}]$ laminate with sensory and active layer.

the generalized equations of motion (16) and (17) and collecting the coefficients, a linear dynamic system of $N+5$ equations effectively results for each mode kl, of the following form:

$$\begin{bmatrix} [M_{uu}]_{kl} & 0 \\ 0 & 0 \end{bmatrix} \begin{Bmatrix} \{\ddot{U}\}_{kl} \\ \{\ddot{\Phi}\}_{kl} \end{Bmatrix} + \begin{bmatrix} [K_{uu}]_{kl} & [K_{u\varphi}]_{kl} \\ [K_{\varphi u}]_{kl} & [K_{\varphi\varphi}]_{kl} \end{bmatrix} \begin{Bmatrix} \{U\}_{kl} \\ \{\Phi\}_{kl} \end{Bmatrix} = \begin{Bmatrix} \{F(t)\}_{kl} \\ \{Q_3(t)\}_{kl} \end{Bmatrix} \tag{19}$$

where $\{U\} = \{U^0, V^0, W^0, \beta_\xi, \beta_\eta\}$ and $\Phi = \{\Phi^1, \ldots, \Phi^N\}$ are the displacement and electric potential amplitude vectors of Eq. (18), $\{F\}_{kl}$ is the Fourier component of the mechanical loads vector, and $\{Q_3\}_{kl}$ is the Fourier component of the surface charge applied to the piezoelectrics. The submatrices K_{uu}, $K_{u\varphi}$, $K_{\varphi\varphi}$ and M_{uu} are equivalent stiffness, piezoelectric, permittivity and mass matrices, respectively, and are calculated from the respective generalized laminate matrices (see Appendix A), for each mode kl.

Assuming the most general case, where some piezoelectric layers of the laminate will be configured as distributed actuators (electric potential applied on both surfaces) and the remaining N^{P} as distributed sensors (electric potential remains free on one surface at least), the electric potential vector is subdivided in a free or sensory component Φ^{P} representing the voltage output at the sensors, and a forced or active component Φ^{A} representing the voltage imposed on the actuator layers, such that $\{\Phi\} = \{\Phi^{\mathrm{P}}; \Phi^{\mathrm{A}}\}$. After partitioning Eq. (19), a set of two linear subsystems, with 5 and N^{P} discrete equations respectively, results for each mode kl of the following form (Saravanos, 1999),

$$[M_{uu}]_{kl}\{\ddot{U}_{kl}\} + [K_{uu}]_{kl}\{U_{kl}\} + [K^{PP}_{u\varphi}]_{kl}\{\Phi^{P}_{kl}\} = \{F_{kl}(t)\} - [K^{PA}_{u\varphi}]_{kl}\{\Phi^{A}_{kl}\} \tag{20}$$

$$[K^{PP}_{\varphi u}]_{kl}\{U_{kl}\} + [K^{PP}_{\varphi\varphi}]_{kl}\{\Phi^{P}_{kl}\} = \{\overline{Q}^{P}_{3kl}(t)\} \tag{21}$$

Eq. (21) describes the linear relationship between modal sensory signal and displacement which, depending on electric conditions imposed on the piezoelectric surfaces, may take the two following different forms. If a sufficiently high electric impedance is connected between the sensor surface terminals (Saravanos, 1999), then $Q^{P}_{3}(t) = 0$ and Eq. (21) takes the form,

$$\{\Phi^{P}_{kl}\} = -[K^{PP}_{\varphi\varphi}]^{-1}_{kl}[K^{PP}_{\varphi u}]_{kl}\{U_{kl}\} \tag{22}$$

that is, the sensory electric potential is directly proportional to the shell displacements. In the other extreme case, when a sufficiently low impedance is connected between the sensor terminals, the electric permittivity charge component becomes negligible. Time differentiation of Eq. (21), yields that in this case, the current density i^{P} between sensor terminals is proportional to the rate of the displacement vector,

$$i^{P}_{kl} = \frac{d}{dt}\{\overline{Q}^{P}_{3kl}(t)\} = [K^{PP}_{\varphi u}]_{kl}\{\dot{U}_{kl}\} \tag{23}$$

3.2. Impactor dynamics

The case of low velocity impact is considered in this work, where rate effects, damage and perforation are neglected. Assuming the case shown in Figs. 1 and 2a where a foreign object of mass m_i, traveling with low velocity v_0 along the ζ axis, transversely impacts the cylindrical shell at a point (ξ_c, η_c), the motion of the impactor is described by

$$m_i\ddot{w}_i(t) = -F_i(t) \tag{24}$$

where w_i is the displacement of the impactor and $F_i(t)$ is the concentrated impact force. The lateral load per unit area applied to the shell is,

$$q_3(\xi,\eta,t) = F_i(t)\delta(\xi - \xi_c)\delta(\eta - \eta_c) \tag{25}$$

For simplicity and without any loss of generality, a linear elastic contact law is used and the impact force $F_i(t)$ is assumed to be,

$$F_i(t) = k_y\alpha(\xi,\eta,t) \tag{26}$$

where, k_y is the local contact stiffness which can be calculated from shell and impactor parameters (Christoforou and Yigit, 1998b), and $\alpha(t)$ is the indentation defined as the relative displacement between the impactor and the shell at the contact point (ξ_c, η_c),

$$\alpha(\xi,\eta,t) = \begin{cases} w_i(t) - w^0(\xi_c,\eta_c,t) & \text{if } w_i(t) - w^0(\xi_c,\eta_c,t) \geqslant 0 \\ 0 & \text{if } w_i(t) - w^0(\xi_c,\eta_c,t) < 0 \end{cases} \tag{27}$$

The previous equations (26) and (27) may be seen as describing the effect of a spring placed between the shell and the impactor as long as both are in contact, which spring pushes the impactor backwards and the shell forwards with a force proportional to the impactor indentation α. The lateral shell displacement w^0 is the summation of all modal contributions as they are provided by the solution of Eqs. (20) and (21) for each mode kl,

$$w^0(\xi,\eta,t) = \sum_k \sum_l W^0_{kl}(t)\sin(a_k\xi)\sin(b_l\eta) \tag{28}$$

The initial conditions of the impact problem are:

$$\begin{aligned} &\{U(\xi,\eta,0)\} = 0, \quad \{\dot{U}(\xi,\eta,0)\} = 0 \\ &w_i(0) = 0 \quad \dot{w}_i(0) = v_0 \end{aligned} \tag{29}$$

3.3. Stress and electric displacement calculation

Although, the mixed-field piezoelectric shell theory is primarily developed for yielding efficient and accurate calculations of global response parameters of thin and intermediately thick shells, it entails also capabilities of stress and electric displacement calculations at various levels of the piezoelectric shell. The mid-strain, curvature and generalized electric field vectors at each point of the shell are provided by Eqs. (A.1), (A.2) and (10), respectively. The in-plane and shear strains through the thickness of the piezo-composite shell are subsequently provided by Eq. (8), while the electric field vector components are predicted by Eq. (9). Finally, local stresses and electric displacements at each through-the-thickness point of the impacted piezolaminate may be calculated from Eq. (1).

It is pointed out, however, that neither damage propagation nor other non-linear effects are considered in this work. Damage in impacted piezolaminates typically involves many different types of failure mechanisms, including delaminations, and its prediction will require stress calculations provided only by refined piezoelectric theories (see e.g., Heyliger and Saravanos (1999)). Yet, all stresses in the shell are proportionally related to the impact force, thus, the prediction (and possible modification) of the impact force history, will also reflect the pattern of stress variation during the impact event. The additional consideration of damage propagation and penetration in the piezoelectric laminate will require rigorous and extensive analytical and experimental developments in many areas, which significantly exceed the scope of this study, and should be considered as topics of future work.

3.4. Numerical solution procedure

The efficient calculation of the impact response, with or without controller interaction, may require substantial computational effort. Eqs. (20), (21) and (24) which describe the modal motion of the shell–impactor system are effectively coupled by the non-linear contact law, Eqs. (26) and (27), thus resulting in a coupled non-linear system potentially of large size. To overcome this, an explicit time integration scheme (based on the central difference method) is used for the solution of the motion equations. Among other benefits, explicit integration schemes calculate the unknown displacements at step $t + \Delta t$ using equilibrium equations at step t, thus the contact equation (27) is effectively imposed at step t, where all modal states are already calculated. The calculated impact force ${}^{t}F$ is then used in Eq. (20) to independently calculate each set of modal state variables ${}^{t+\Delta t}\{U\}_{kl}$, ${}^{t+\Delta t}\{\Phi\}^{\mathrm{P}}_{kl}$, ${}^{t+\Delta t}w_i$ of the shell–impactor system. In this manner, the equations are numerically uncoupled, and a small set of modal motion equations is independently solved at each time step for each mode, with obvious computational advantages.

4. Active impact control

An obvious application of piezoelectric shells may be in active impact control. In this concept, the performance of the impacted structure may be improved by feeding back to piezoelectric actuators, either the state variables, or the output signals of piezoelectric sensors. Impact force control rather than vibration control is sought, as impact force is considered to be directly related to shell stresses. In this context, impact force minimization may implicitly lead to impact damage mitigation and increased post-impact residual strength. Thus, the development of adaptive piezoelectric shells for active impact control involves substantial differences and challenges because of the introduction of additional state variables by the impactor, the non-linearity of the plant system, the consideration of impact force as primary control objective, and the extension–bending coupling effect induced on actuators and sensors by the shell geometric curvature (Eq. (2)).

Apparently, the development of such adaptive shells and controllers may be a topic requiring substantial effort, thus the present work should be viewed as a first attempt to investigate the feasibility of the concept. It is interesting, therefore, to examine if the impact force may be controlled with piezoelectric actuators using two types of control feedback: state feedback; and output feedback from piezoelectric sensors. The possibility to design a successful controller using a simplified linear shell–impactor system is also evaluated. The governing equations of the shell–impactor system may be cast in standard state space system form:

$$\begin{aligned} \dot{\boldsymbol{x}} &= f(\boldsymbol{x}, t) + [B]\boldsymbol{u} \\ \boldsymbol{y} &= [C]\boldsymbol{x} \end{aligned} \tag{30}$$

where, the first equation contains the non-linear equations of motion, as mandated by condensed Eqs. (20), (21) and (24); the second equation describes the relation of sensory signal (output) to the state, using either of Eq. (22) or (23). The state vector $\boldsymbol{x}$ includes the amplitudes of the modal velocities and displacements of the shell, and of the velocity and position of the impactor $\boldsymbol{x} = \{\dot{\boldsymbol{U}}_{\boldsymbol{11}}, \boldsymbol{U}_{\boldsymbol{11}}, \ldots, \dot{\boldsymbol{U}}_{\boldsymbol{mn}}, \boldsymbol{U}_{\boldsymbol{mn}}, \dot{w}_i, w_i\}$; the input vector $\boldsymbol{u}$ includes the modal voltage amplitudes applied on the active layers, $\boldsymbol{u} = \{\varphi^A_{11}, \ldots, \varphi^A_{mn}\}$; and the output vector $\boldsymbol{y}$ contains either the modal potential or the modal current density amplitudes of the sensor layers. While the above equations describe the actual plant system, a simplified linear system is also considered for controller design purposes, with identical equations of motion, except that Eq. (27) is neglected, i.e. a contact force is always applied on the shell irrespectively of the sign of identation α,

$$\begin{aligned} \dot{\boldsymbol{x}} &= [A]\boldsymbol{x} + [B]\boldsymbol{u} \\ \boldsymbol{y} &= [C]\boldsymbol{x} \end{aligned} \tag{31}$$

4.1. State feedback control

In this case, the input to piezoelectric actuators is proportional to the state variables,

$$\boldsymbol{u} = -[G_x]\boldsymbol{x} \tag{32}$$

where $[G_x]$ is a gain matrix, describing the controller. A linear quadratic regulator (LQR) may be designed with optimal gains, such that a performance index J with quadratic terms on the state and control effort is minimized,

$$J = \frac{1}{2}\int_0^\infty (\boldsymbol{x}^{\mathrm{T}}[Q]\boldsymbol{x} + \boldsymbol{u}^{\mathrm{T}}[R]\boldsymbol{u})\,\mathrm{d}t \tag{33}$$

where $[Q]$ and $[R]$ are weighting matrices. An optimal LQR provides the best closed-loop performance. However, an LQR controller may be impractical to implement as it requires knowledge of all states, including impactor position and velocity. The optimal gain matrix is calculated for the simplified linear plant system (31), solving a matrix Riccati equation (see, Sage and White (1977)). This gain matrix is subsequently used as the controller of the actual non-linear plant system (30).

4.2. Output feedback control

In this case, the input to piezoelectric actuators is proportional to the system output, which includes only signals from piezoelectric sensors,

$$\boldsymbol{u} = -[G_y]\boldsymbol{y} \tag{34}$$

where $[G_y]$ is a proper gain matrix. While an output feedback controller is simpler to implement, its development is usually more cumbersome. Formal development of an output feedback controller is possible

using either a state estimator or direct prediction of an optimum gain matrix, all in connection with the minimization of the performance index J. This paper mainly investigates the feasibility of sensory feedback by trying simple gain matrices, whereas the formal design of an optimized output controller is left as a topic of future work.

5. Evaluations and discussion

Numerical results and case studies are presented which evaluate the formulation and quantify the impact response of adaptive piezoelectric shells. The response of $[p^{\mathrm{P}}/(0/90)_2/0]_{\mathrm{s}}$ Gr/Epoxy cylindrical panels of various curvatures with symmetrically attached piezoelectric sensors is evaluated (Fig. 2b). Letter p is used in the standard laminate notation to indicate a *piezoelectric* layer, either in sensory (superscript P) or in active (superscript A) configuration. The active impact control of a $[(0/90)_2/0_2/(90/0)_2/p^{\mathrm{P}}/p^{\mathrm{A}}]$ Gr/Epoxy shell with state and output feedback is also considered (Fig. 2c). For convenience, a common piezoceramic material (PZT-4) was considered in all examples. All shells are impacted at the centers ($\xi/L_\xi = \eta/L_\eta = 0.5$) of their convex surface ($\zeta = +h/2$) by impactors traveling perpendicularly to the surface towards the center of curvature. The dimensions of all panels were assumed to be $L_\xi = L_\eta = 200$ mm and the thickness of each composite ply was 0.270 mm. The material properties are shown in Table 1.

5.1. Sensory cylindrical panels

The impact response of $[p^{\mathrm{P}}/(0/90)_2/0]_{\mathrm{s}}$ Gr/Epoxy cylindrical panels with symmetrically attached piezoceramic (PZT-4) sensory layers (see Fig. 2b) was evaluated. The edge dimensions of all panels were as-

Table 1
Mechanical properties ($\varepsilon_0 = 8.85 \times 10^{-12}$ farad/m, electric permittivity of air)

Property	Gr/Epoxy	PZT-4
Elastic properties		
E_{11} (GPa)	120	81.3
E_{22} (GPa)	7.9	81.3
E_{33} (GPa)	7.9	64.5
G_{23} (GPa)	5.5	25.6
G_{13} (GPa)	5.5	25.6
G_{12} (GPa)	5.5	30.6
v_{12}	0.3	0.33
v_{13}	0.3	0.43
v_{23}	0.3	0.43
Piezoelectric coefficients (10^{-12} m/V)		
d_{31}	0	−122
d_{32}	0	−122
d_{24}	0	495
d_{15}	0	495
Electric permittivity		
$\varepsilon_{11}/\varepsilon_0$	3.5	1475
$\varepsilon_{22}/\varepsilon_0$	3.0	1475
$\varepsilon_{33}/\varepsilon_0$	3.0	1300
Mass density (kg/m^3)		
ρ	1578	7600
Contact stiffness (MN/m)		
k_y	12.34	12.34

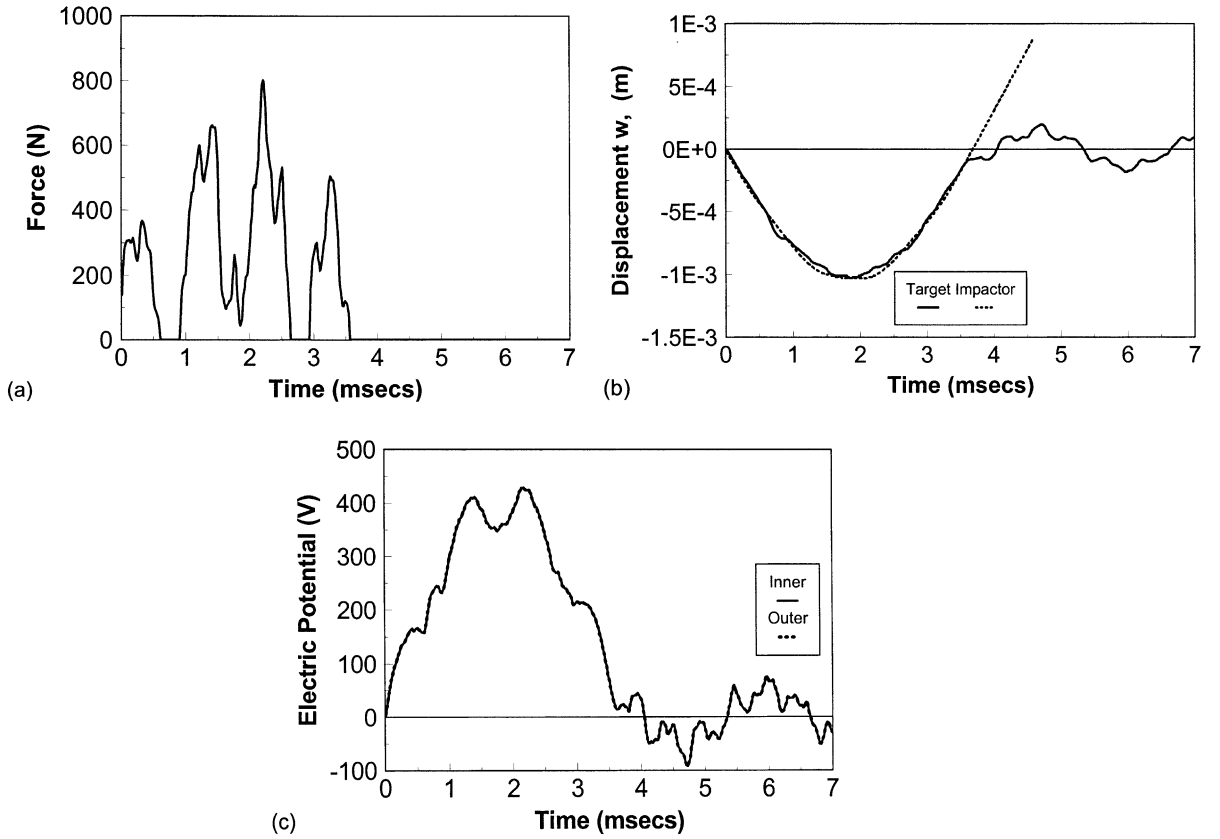

Fig. 3. Impact of $[p^{P}/(0/90)_2/0]_s$ simply supported piezoelectric composite plate ($1/R_1 = 0$) by a 0.5 kg, 1 m/s impactor. (a) Impact force, (b) displacement at center, (c) voltage at inner and outer sensor at center of panel.

sumed to remain the same $L_\xi = L_\eta = 200$ mm, yet, the curvature ($1/R_1$) of each panel was varied to investigate the effect of curvature on impact response. The thickness of each piezoceramic sensor layer was 0.250 mm. Various mass impactors were considered, all traveling with an initial velocity of 1 m/s.

Figs. 3–6 show impacts with a 0.5 kg impactor on panels of zero curvature ($1/R_1 = 0$ or $\theta = 0°$), low curvature ($1/R_1 = 1.309$ or $\theta = 15°$), intermediate curvature ($1/R_1 = 3.927$ or $\theta = 45°$) and high curvature ($1/R_1 = 15.708$ or $\theta = 180°$), respectively. Each figure presents: (a) the predicted impact force (in absolute value), (b) the panel and impactor displacement, and (c) the sensory voltages of the inner and outer sensory layers at the center ($\xi/L_\xi = \eta/L_\eta = 0.5$) of the panel. Clearly, the change of curvature has a profound effect on the impact response of the panel. As the curvature of the panel increases, the impact characteristics and impact force seem to change drastically. The multiple impacts predicted here and in subsequent cases, are indicative of the impactor "spring-back" effect provided by Eqs. (26) and (27). The multiple impacts observed in the panels of zero or low curvature do progressively change to a single impact of shorter duration and higher force at the higher curvature panels. This is primarily attributed to the increase of effective stiffness with curvature due to increased coupling between extension and flexure. The effect of stiffening is also depicted on the reduction of shell and impactor displacements, as the panel curvature increases. Another factor contributing to the change of impact characteristics at high curvature panels, is that higher mode shapes, i.e. modes of shorter semi-wavelength such as $(2,1)$ and $(3,1)$, appear at lower modal frequencies, while the fundamental mode shape $(1,1)$ shifts to higher ones. The shifting of higher mode shapes

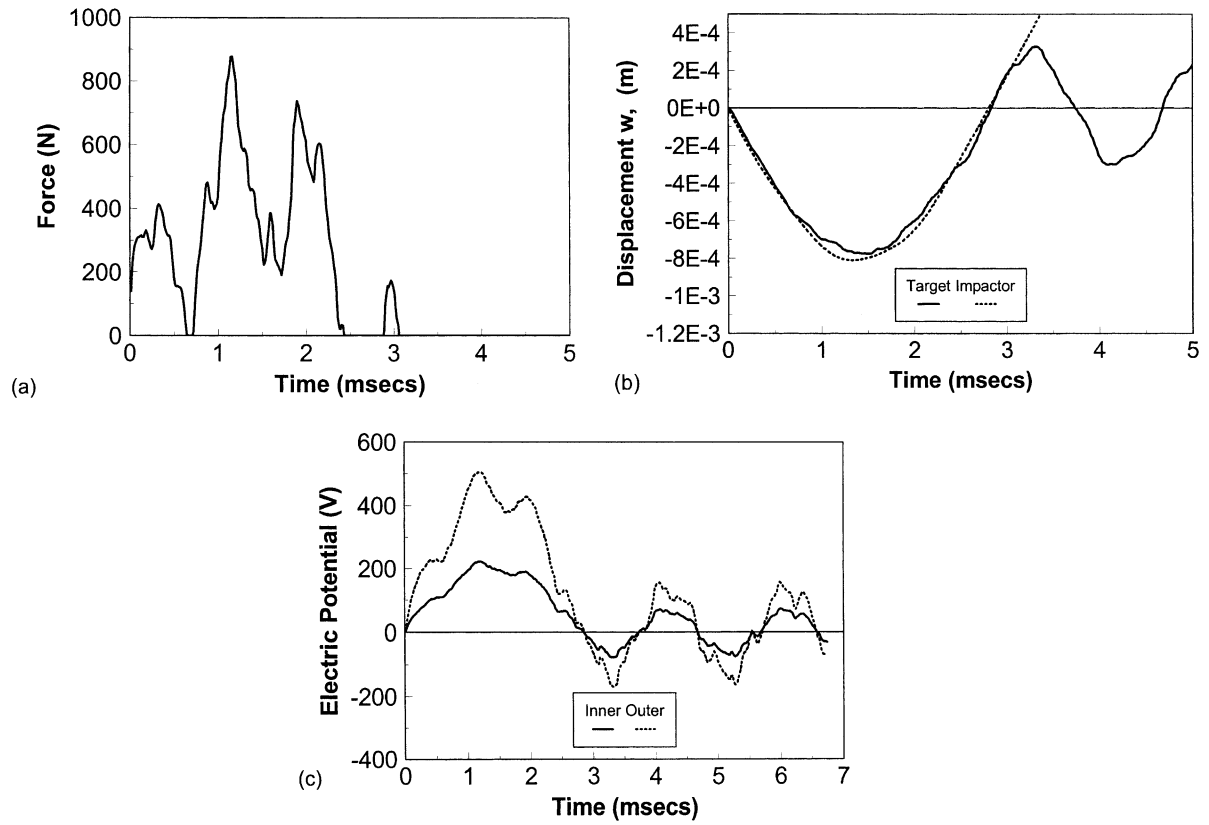

Fig. 4. Impact of $[p^{P}/(0/90)_2/0]_s$ simply supported low curvature cylindrical piezoelectric composite panel ($1/R_1 = 1.309$) by a 0.5 kg, 1 m/s impactor. (a) Impact force, (b) displacement at center, (c) voltage at inner and outer sensor at center of panel.

in the lower natural frequency range, also contributes to the localization of the impact in the high curvature panels.

Figs. 3c–6c show the predicted electric potential response at the free terminals of the inner and outer sensor (see Fig. 2b). The predicted electric potential at both sensors seems to encompass trends of both force and displacement responses. This seems to occur irrespectively of the panel curvature. Yet, different voltage signals will develop at the inner and outer sensors at non-zero curvatures. While both sensors provided exactly the same voltage in the case of the flat panel ($1/R_1 = 0$) as seen in Fig. 3c, the voltage signal of the inner and outer sensor begin to take progressively different values as the panel curvature increases (see Figs. 4c–6c). At high curvatures, the sensory signals have virtually opposite polarity. Apparently, strong mid-surface extensional strains develop at non-zero curvatures as mandated by Eq. (A.1), thus, bending and extensional strains coexist in the cylindrical laminate. The resulting non-symmetric strain variation through the thickness, yields the non-symmetric sensory voltages shown in Figs. 4c–6c.

The previous impactor mass was selected, such that, for the plate case ($1/R_1 = 0$) the impactor–structure system will fall in the transition area between local and global (quasi-static) stiffness dominated impacts (Christoforou and Yigit, 1998b). The effect of impactor mass on cylindrical piezoelectric shells was further evaluated, by considering the extreme cases of heavy (5 kg) and light (0.008 kg) impactors which in the case of the flat panel yield impacts in the global and local stiffness predominant regimes, respectively. The resultant force applied by the 5 kg impactor on cylindrical panels of low, intermediate and high curvature is

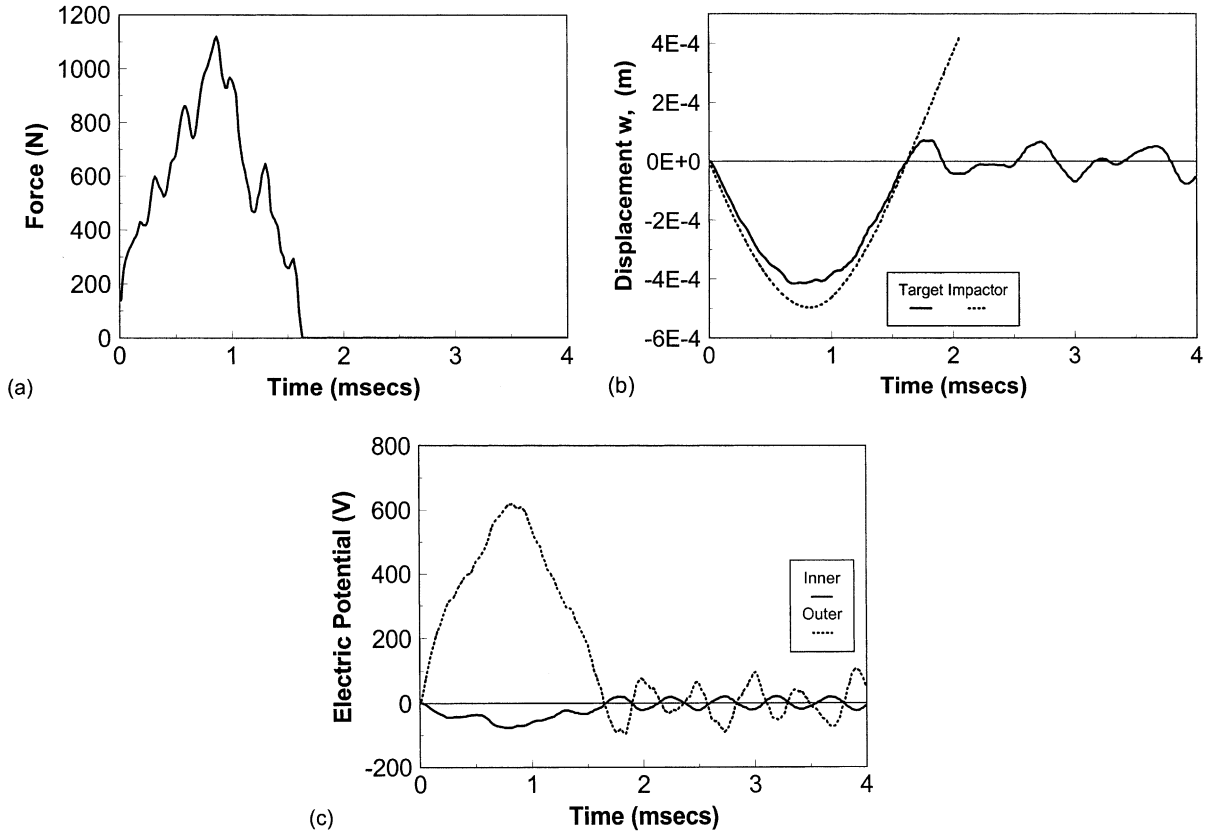

Fig. 5. Impact of $[p^{P}/(0/90)_2/0]_s$ simply supported intermediate curvature cylindrical piezoelectric composite panel ($1/R_1 = 3.927$) by a 0.5 kg, 1 m/s impactor. (a) Impact force, (b) displacement at center, (c) voltage at inner and outer sensor at center of panel.

shown in Fig. 7. This heavy impactor produces quasi-static impacts in the case of zero and low curvature panels. The increasing curvature of the panel has a significant effect on impact response, resulting in impact forces having shorter duration, higher force magnitude and lower interactions between the impactor and the shell. The sensory voltage shown in Fig. 8 seems to follow again the trend between impact force and shell displacement, yet, the signals in the two sensors differ significantly at the higher curvature panels.

Finally, the predicted impact force in the case of a light mass (0.008 kg) impactor is shown in Fig. 9. Single impacts of short duration were predicted for all curvatures and the effect of curvature on the impact force was minor. These impacts are mostly controlled by the local stiffness coefficient k_y which was assumed to be independent of the curvature at the point of contact, whereas, the participation of the global shell stiffness is rather insignificant. The sensory signal, mostly followed the transient displacement of the shell. The effect of curvature and through-thickness sensor position on sensory voltage, although not shown, was found to be significant as in the case of heavier mass impacts.

Overall, the previous results have shown that the signal of the piezoelectric sensors may be good indicators of force and shell deflection. Yet, all results have shown strong interdependence between sensory signals and shell curvature suggesting that both interpretation and use of sensory signals in shell structures may require special consideration, thus, highlighting the value of the present formulation. Finally, the predicted high sensory signals suggest that a wide variety of piezoelectric materials with lower piezoelectric

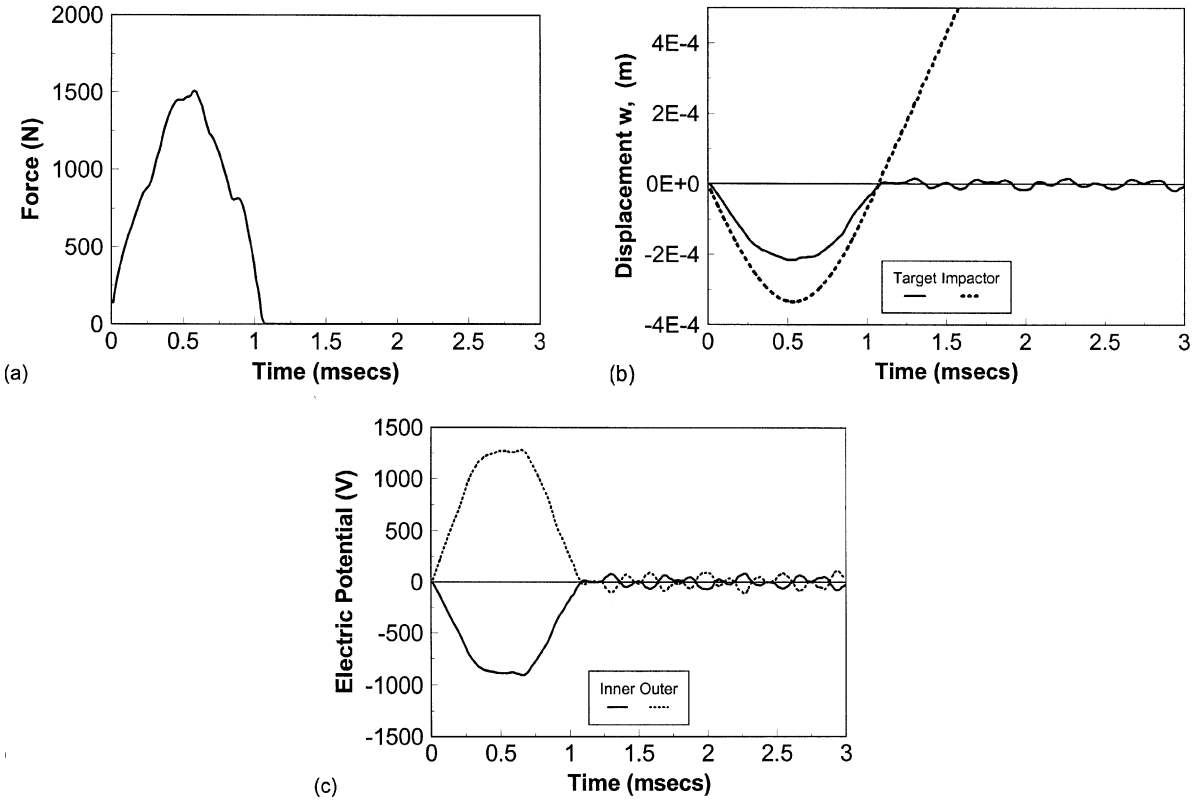

Fig. 6. Impact of $[p^{P}/(0/90)_2/0]_s$ simply supported high curvature cylindrical piezoelectric composite panel ($1/R_1 = 15.708$) by a 0.5 kg, 1 m/s impactor. (a) Impact force, (b) displacement at center, (c) voltage at inner and outer sensor at center of panel.

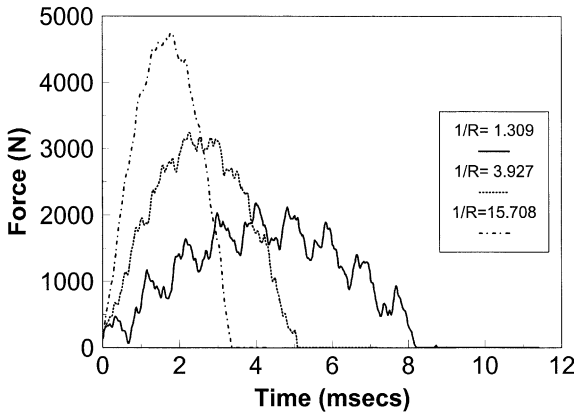

Fig. 7. Impact force on $[p^{P}/(0/90)_2/0]_s$ simply supported cylindrical piezoelectric composite panels of various curvatures, impacted by a heavy (5 kg, 1 m/s) impactor.

stress coefficients may be used as sensors, among them piezopolymers (i.e. PVDF) which exhibit superior impact toughness and shape conformity.

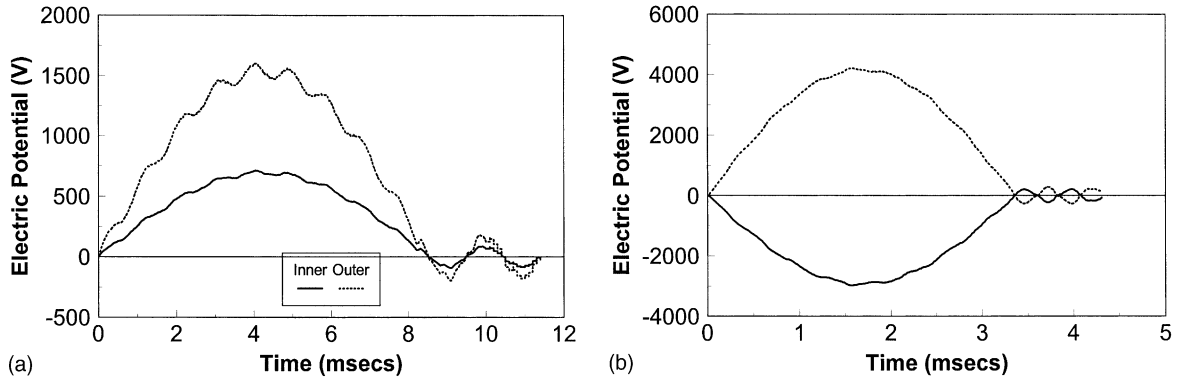

Fig. 8. Sensory voltage at inner and outer sensor at the center of cylindrical $[p^{P}/(0/90)_2/0]_s$ simply supported panels impacted by a heavy (5 kg, 1 m/s) impactor. (a) Low curvature $1/R_1 = 1.309$, (b) high curvature ($1/R_1 = 15.708$).

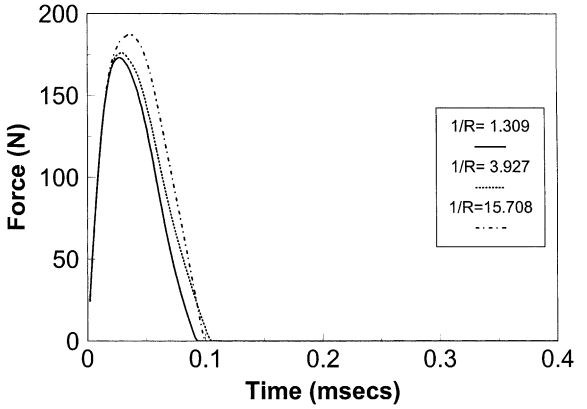

Fig. 9. Impact force on $[p^{P}/(0/90)_2/0]_s$ simply supported cylindrical piezoelectric composite panels of various curvatures, impacted by a light (0.008 kg, 1 m/s) impactor.

5.2. Active impact control

The active impact control of $[(0/90)_2/0_2/(90/0)_2/p^{P}/p^{A}]$ Gr/Epoxy shells impacted by a 0.5 kg impactor at the center of their outer (convex) surface was studied (see Fig. 2c). A 0.125 mm sensor and 0.250 mm actuator layer were attached at the inner (concave) surface of the shell. For simplicity, the system response was approximated using the first 3×3 mode shapes. The equations of motion and the rotations were further condensed to the three modal displacements, $\{U\}_{kl} = \{U^0, V^0, W^0\}_{kl}$, by assuming negligible rotational inertias. Only the odd modes $(1,1)$, $(1,3)$, $(3,1)$ and $(3,3)$ are excited by the impactor force, thus, the shell–impactor system effectively involved 26 state variables, of which 24 describe the modal velocities and deflections of the shell. The system inputs were the amplitudes of the modal electric potential applied to the active layer, $\boldsymbol{u} = \{\varphi^{A}_{11}, \varphi^{A}_{13}, \varphi^{A}_{31}, \varphi^{A}_{33}\}$. The amplitudes of the electric potential at the the free sensor terminal were the system output.

5.2.1. Optimal state-feedback control

An optimal LQR controller was designed using the simplified linear system (Eq. (31)) of the previous model. The weighting matrices $[Q]$ that were used, had the form $\boldsymbol{x}^{T}[Q]\boldsymbol{x} = c_1(\dot{w}^0 - \dot{w}_i)^2 + c_2(w^0 - w_i)^2$,

where the first quadratic term represents a measure of the rate of indentation (and also, of the momentum difference between shell and impactor), while the second term is a measure of indentation (and also of the impact force). The weighting matrix $[R]$ on the control effort term was set to be a unity matrix. Optimal feedback gain matrices $[K_x^*]$ were calculated for the linear system (31) and were subsequently used as the controller of the actual non-linear system (30). The maximum values of c_1 and c_2 were selected such that the modal amplitudes of actuator input remained approximately within the ± 250 V range.

Fig. 10 shows the reduction of impact force in a low curvature shell ($1/R_1 = 1.309$ or $\theta = 15°$) obtained with optimal LQR controllers attempting to minimize either the rate of indentation, or the impact force for the duration of the impact. For minimal rate of indentation (controller LQR1), the weighting matrix $[Q]$ corresponded to weighting factors $c_1 = 300 \times 10^3$ and $c_2 = 0$, while for minimal impact force (controller LQR2) the factors $c_1 = 0$ and $c_2 = 300 \times 10^3$ were used. Clearly both controllers have obtained significant reductions in the impact force. Fig. 11 shows the corresponding shell and impactor displacement for the shell, (a) without control and (b) with LQR2. The reduction of impact force was primarily obtained by eliminating the contribution of higher modes, thus obtaining smoother contact between shell and impactor. Fig. 12 shows the impact force for an intermediate curvature shell ($1/R_1 = 3.927$ or $\theta = 45°$) with LQR controllers designed with identical weighting matrices $[Q]$ as in the previous example. The controlled panels have reduced the impact force, however, the reduction is smaller than the previous case. As seen in Fig. 13,

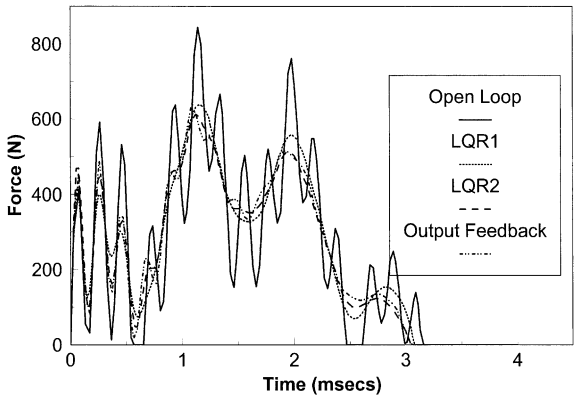

Fig. 10. Impact force of actively controlled $[(0/90)_2/0_2/(90/0)_2/p^P/p^A]$ low curvature cylindrical piezoelectric composite panels ($1/R_1 = 1.309$) with various controllers. 0.5 kg, 1 m/s impactor.

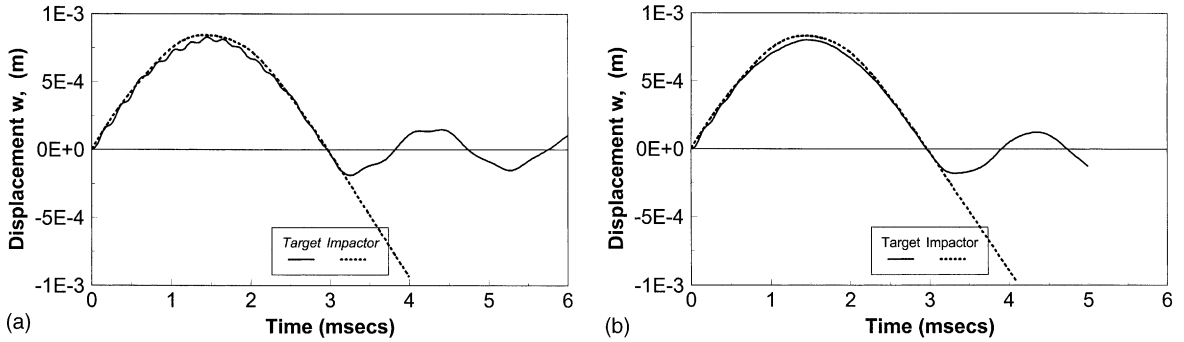

Fig. 11. Displacements of an actively controlled $[(0/90)_2/0_2/(90/0)_2/p^P/p^A]$ low curvature cylindrical piezoelectric composite panels ($1/R_1 = 1.309$). (a) Without controller interaction, (b) with state feedback (LQR2) controller. 0.5 kg, 1 m/s impactor.

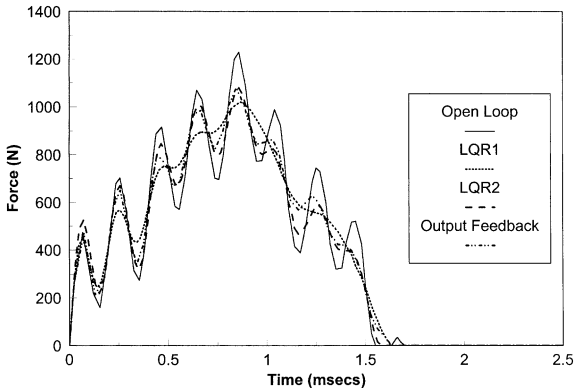

Fig. 12. Impact force of actively controlled $[(0/90)_2/0_2/(90/0)_2/p^P/p^A]$ intermediate curvature cylindrical piezoelectric composite panels ($1/R_1 = 3.927$) with various controllers. 0.5 kg, 1 m/s impactor.

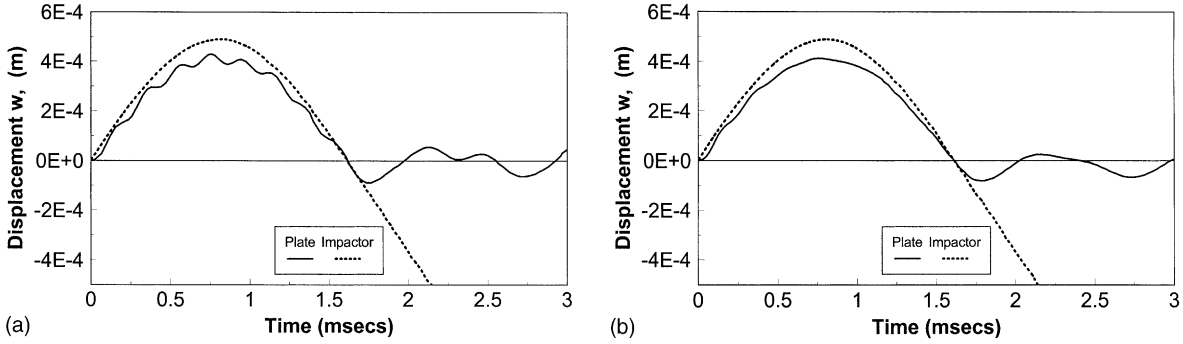

Fig. 13. Displacements of an actively controlled $[(0/90)_2/0_2/(90/0)_2/p^P/p^A]$ intermediate curvature cylindrical piezoelectric composite panels ($1/R_1 = 3.927$). (a) Without controller interaction, (b) with state feedback (LQR1) controller. 0.5 kg, 1 m/s impactor.

the elimination of higher mode contributions continued to be the mechanism for reducing the impact force. The participation of higher modal shapes in the impact, as well as the more localized nature of the impact due to membrane stiffening, have both reduced the effectiveness of the active layer.

5.2.2. Output feedback control

The feasibility of an output feedback controller was also investigated. The system output was considered to be the modal current densities of the piezoelectric sensor (Eq. (23)), $\boldsymbol{y} = (i^P_{11}, i^P_{13}, i^P_{31}, i^P_{33})$. A diagonal matrix of uniform gains $[K_y] = \mathrm{diag}(k, \ldots, k)$ was tried with $k = 50$. The resultant impact forces are shown respectively in Figs. 10 and 12, for both shells. In both cases, the results illustrate the feasibility to reduce impact force using direct sensor feedback to the piezoelectric actuators. Moreover, the obtained reductions seem comparable with those obtained by the LQR controllers.

Overall, the previous case studies have shown the feasibility, but also the limitations, of active impact control in adaptive shells of low and intermediate curvatures for medium mass impactors (impacts in the local–global transitional area) using piezoceramic actuators. An emerging issue now is the capability of piezoelectric actuators to survive the impact event; this may be addressed in the future either by proper

piezoelectric material selection and development, or by proper actuator placement. In both cases, the value of the present method in predicting the impact response and configuring and optimizing the elements of an adaptive piezoelectric shell is obvious.

6. Summary

The theoretical framework for analyzing low-energy impacts on laminated shells of double curvature with distributed piezoelectric actuator and sensor layers were formulated, including impactor dynamics and contact law. The formulation encompasses a coupled piezoelectric shell theory with first order shear kinematic assumptions for displacements and layerwise electric potential variation. Exact in-plane Ritz solutions were formulated for analyzing the impact of open cylindrical piezoelectric–composite shells. Although the modal shell equations are physically coupled by the contact law, the modal equations of motion where numerically decoupled and solved using explicit time integration. The active impact control problem using piezoelectric actuators was also addressed using either an optimized state feedback controller proposed to be designed based on simplified linear dynamics of the shell–impactor, or output feedback from piezoelectric sensors.

Numerical results for the impact response of cross-ply graphite/epoxy simply supported shells of various curvatures with surface bonded piezoceramic sensors were presented. Impact force, displacement and sensor responses were predicted. Various mass impactors were also studied. Among other things, the results have shown the significant dependence of impact force and sensory voltage on shell curvature. As the curvature increased, there was a clear trend for formation of single impacts with "sinusoidal" impact force patterns. In all cases the sensory voltage seemed to provide an indication of impact force trajectory, yet, the sign and magnitude of sensory voltage were strongly related to the shell curvature. The feasibility of active impact control was also studied. It was predicted that for at least medium mass impactors (local–global transition), impact force reductions may be attained in shells of low and intermediate curvature using piezoelectric actuators with LQR state feedback controllers or output feedback controllers based on piezoelectric sensor current. The output controller yielded comparable force reductions to the optimal LQR controller. The case studies have shown the feasibility, but also the limitations, of active impact control in adaptive shells of low and intermediate curvatures. Overall, the results have demonstrated the capabilities of the developed mechanics and analytical models to quantifying the impact response of adaptive cylindrical piezoelectric composite shells. Future studies may directly quantify the effect of impact force reduction on impact energy absorption, damage mitigation and post impact residual strength of adaptive piezoelectric shells.

Appendix A

Generalized laminate strain and curvature,

$$
\begin{aligned}
S_1^0 &= \frac{1}{g_{11}^0}\left(u_{,\xi}^0 + \frac{g_{11,\eta}^0}{g_{22}^0}v^0\right) + \frac{w^0}{R_1}, \quad S_2^0 = \frac{1}{g_{22}^0}\left(v_{,\eta}^0 + \frac{g_{22,\xi}^0}{g_{11}^0}u^0\right) + \frac{w^0}{R_2} \\
S_6^0 &= \frac{1}{g_{11}^0}\left(v_{,\xi}^0 - \frac{g_{11,\eta}^0}{g_{22}}u^0\right) + \frac{1}{g_{22}^0}\left(u_{,\eta}^0 - \frac{g_{22,\xi}^0}{g_{11}}v^0\right) \\
S_4^0 &= \beta_\eta + \frac{w_{,\eta}^0}{g_{22}^0} - \frac{v^0}{R_2}, \quad S_5^0 = \beta_\xi + \frac{w_{,\xi}^0}{g_{11}^0} - \frac{u^0}{R_1}
\end{aligned}
\tag{A.1}
$$

$$k_1 = \frac{1}{g_{11}^0}\left(\beta_{\xi,\xi} + \frac{g_{11,\eta}^0}{g_{22}^0}\beta_\eta\right), \quad k_2 = \frac{1}{g_{22}^0}\left(\beta_{\eta,\eta} + \frac{g_{22,\xi}^0}{g_{11}^0}\beta_\xi\right)$$
$$k_6 = \frac{1}{g_{11}^0}\left(\beta_{\eta,\xi} - \frac{g_{11,\eta}^0}{g_{22}^0}\beta_\xi\right) + \frac{1}{g_{22}^0}\left(\beta_{\xi,\eta} - \frac{g_{22,\xi}^0}{g_{11}^0}\beta_\eta\right) \tag{A.2}$$

Generalized constitutive laminate equations,

$$N_i = A_{ij}S_j^0 + B_{ij}k_j^0 - \sum_{m=1}^{N}\overline{E}_{3l}^m E_3^m, \quad i,j = 1,2,6$$
$$N_i = A_{ij}S_j^0 - \sum_{m=1}^{N}\overline{E}_{ik}^m E_k^m, \quad i,j = 4,5 \;\; k = 1,2 \tag{A.3}$$
$$M_i = B_{ij}S_j^0 + D_{ij}k_j^0 - \sum_{m=1}^{N}\hat{E}_{3l}^m E_3^m, \quad i,j = 1,2,6$$

$$D_i^m = \overline{E}_{ij}^m S_j^0 + \sum_{n=1}^{N} G_{ii}^{mn}E_i^n, \quad i = 1,2, \;\; j = 4,5$$
$$D_3^m = \overline{E}_{3j}S_j^0 + \hat{E}_{3j}k_j^0 + \sum_{n=1}^{N} G_{33}^{mn}E_3^n, \quad j = 1,2,6 \tag{A.4}$$

Equivalent laminate stiffness matrices [A], [B], and [D],

$$\langle A_{ij}, B_{ij}, D_{ij}\rangle = g_{11}^0 g_{22}^0 \sum_{l=1}^{L}\int_{\zeta_l}^{\zeta_{l+1}} C_{ij}\langle 1,\zeta,\zeta^2\rangle \,\mathrm{d}\zeta, \quad i,j = 1,2,6$$
$$A_{ij} = g_{11}^0 g_{22}^0 \sum_{l=1}^{L}\int_{\zeta_l}^{\zeta_{l+1}} C_{ij}\,\mathrm{d}\zeta, \quad i,j = 4,5, \tag{A.5}$$

piezoelectric laminate matrices [E^m] overbar and overhat,

$$\langle \overline{E}_{ij}^m, \hat{E}_{ij}^m\rangle = g_{11}^0 g_{22}^0 \sum_{l=1}^{L}\int_{\zeta_l}^{\zeta_{l+1}} e_{ij}\Psi_{,\zeta}^m(\zeta)\langle 1,\zeta\rangle \,\mathrm{d}\zeta, \quad i = 3, \;\; j = 1,2,6$$
$$\overline{E}_{ij}^m = g_{11}^0 g_{22}^0 \sum_{l=1}^{L}\int_{\zeta_l}^{\zeta_{l+1}} e_{ij}\Psi^m(\zeta)\,\mathrm{d}\zeta, \quad i = 1,2, \;\; j = 4,5 \tag{A.6}$$

and matrices of electric permittivity [G^{mn}],

$$G_{ii}^{mn} = g_{11}^0 g_{22}^0 \sum_{l=1}^{L}\int_{\zeta_l}^{\zeta_{l+1}} \varepsilon_{ii}\Psi^m(\zeta)\Psi^n(\zeta)\,\mathrm{d}\zeta$$
$$G_{33}^{mn} = g_{11}^0 g_{22}^0 \sum_{l=1}^{L}\int_{\zeta_l}^{\zeta_{l+1}} \varepsilon_{33}\Psi_{,\zeta}^m(\zeta)\Psi_{,\zeta}^n(\zeta)\,\mathrm{d}\zeta \tag{A.7}$$

where, L is the number of plies in the laminate.

Generalized densities ρ^A, ρ^B, ρ^D expressing the mass, mass coupling and rotational inertia of the laminate, respectively,

$$\langle \rho^A, \rho^B, \rho^D \rangle = g_{11}^0 g_{22}^0 \sum_{l=1}^{L} \int_{\zeta_l}^{\zeta_{l+1}} \rho_l \langle 1, \zeta, \zeta^2 \rangle \, \mathrm{d}\zeta \tag{A.8}$$

References

Abramovich, H., 1998. Deflection control of laminated beams with piezoceramic layers-closed form solutions. Composite Structures 43, 27–231.

Baz, A., Poh, S., 1988. Performance of an active control system with piezoelectric actuators. Journal of Sound and Vibration 126 (2), 327–343.

Birman, V., Chantrashekhara, K., Sukhendu, S., 1997. Global strength of hybrid shape memory composite plates subjected to low-velocity impact. Journal of Reinforced Plastics and Composites 16 (9), 791–809.

Cairns, D.S., Lagace, P.A., 1989. Transient response of graphite/epoxy and kevlar/epoxy laminates subject to impact. AIAA Journal 27 (11), 1590–1596.

Chantrashekhara, K., Agarwal, A.N., 1993. Active vibration of laminated composite plates using piezoelectric devices: a finite element approach. Journal of Intelligent Material Systems and Structures 4 (4), 496–508.

Choi, K., Chang, F.K., 1996. Identification of impact force and location using distributed sensors. AIAA Journal 34 (1), 136–142.

Christoforou, A.P., Swanson, S.R., 1990. Analysis of simply-supported orthotropic cylindrical shells subject to lateral impact loads. ASME Journal of Applied Mechanics 57, 376–382.

Christoforou, A.P., Swanson, S.R., 1991. Analysis of impact response in composite plates. International Journal of Solids and Structures 27 (2), 161–170.

Christoforou, A.P., Yigit, A.S., 1998a. Effect of flexibility on low velocity impact response. Journal of Sound and Vibration 217 (3), 563–578.

Christoforou, A.P., Yigit, A.S., 1998b. Characterization of impact in composite structures. Composite Structures 43, 15–24.

Kokonis, D.B., Kollar, L.P., Springer, G.S., 1994. Shape control of composite plates with embedded actuators. I. Voltages specified. Journal of Composite Materials 28 (5), 415–458.

Librescu, L., Na, S., 1998. Dynamic response control of thin-walled beams to blast pulses using structural tailoring and piezoelectric actuation. ASME Journal of Applied Mechanics 65, 497–504.

Liu, G.R., Peng, X.Q., Lam, K.Y., Tani, J., 1999. Vibration control simulation of laminated composite plates with integrated piezoelectrics. Journal of Sound and Vibration 220 (5), 827–846.

Matemilola, S.A., Stronge, W.J., 1997. Impact response of composite cylinders. International Journal of Solids and Structures 34 (21), 2669–2684.

Pierson, M.O., Vaziri, R., 1996. Analytical solution for low-velocity impact response of composite plates. AIAA Journal 34 (8), 1633–1640.

Prasad, C.B., Ambur, D.R., Starnes Jr., J.H., 1994. Response of laminated composite plates to low velocity impact by different impactors. AIAA Journal 32 (6), 1270–1277.

Qian, Y., Swanson, S.R., 1990. Experimental measurement of impact response in carbon/epoxy plates. AIAA Journal 28 (6), 1069–1074.

Ray, M.C., 1998. Optimal control of laminated plate with piezoelectric sensor and actuator layers. AIAA Journal 36 (12), 2204–2208.

Sage, A.P., White, C.C., 1977. Optimum Systems Control. Prentice Hall, Englewood Hills, NJ.

Sankar, B.V., Sun, C.T., 1985. Low-velocity impact response of laminated beams subjected to initial stresses. AIAA Jounal 23 (12), 1962–1969.

Saravanos, D.A., 1997. Coupled mixed-field laminate theory and finite element for smart piezoelectric composite shell structures. AIAA Journal 35 (8), 1327–1333.

Saravanos, D.A., 1999. Damped vibration of composite plates with passive piezoelectric-resistor elements. Journal of Sound and Vibration 221 (5), 867–885.

Saravanos, D.A., Christoforou, A.P., 2000. Impact response of adaptive piezoelectric laminated plates. In: Proceedings of the 41st AIAA/ASME/ASCE/AHS/ASC Structures, Structural Dynamics, and Materials Conference, 3–6 April 2000, Atlanta, GA, Paper No. AIAA 2000-1498 (also in press AIAA Journal).

Saravanos, D.A., Heyliger, P.R., 1999. Mechanics and computational models for laminated piezoelectric beams, plates and shells. Applied Mechanics Reviews 52 (10), 305–320.

Soedel, W., 1993. Deep Shell Equations, Vibrations of Shells and Plates. Marcel Dekker, New York.

Sunar, M., Rao, S.S., 1999. Recent advances in sensing and control of flexible structures via piezoelectric materials technology. Applied Mechanics Reviews 52 (1), 1–16.

Swanson, S.R., Smith, N.L., Qian, Y., 1991. Analytical and experimental strain response in impact of composite cylinders. Composite Structures 18, 95–108.

Tracy, M., Chang, F.K., 1998. Identifying impacts in composite plates with piezoelectric strain sensors. Part I: Theory. Journal of Intelligent Material Systems and Structures 9, 920–928.

Tzou, H.S., Tseng, C.I., 1990. Distributed piezoelectric sensor/actuator design for dynamic measurement/control of distributed parameter systems: a piezoelectric finite element approach. Journal of Sound and Vibration 138 (1), 17–34.

Tzou, H.S., Zhong, J.P., 1993. Electromechanics and vibrations of piezoelectric shell distributed systems. Journal of Dynamic Systems Measurement and Control 115 (3), 506–517.

Vaziri, R., Quan, X., Olson, M.D., 1996. Impact analysis of laminated composite plates and shells by super finite elements. International Journal of Impact Engineering 18 (7/8), 765–782.

Yigit, A.S., Christoforou, A.P., 1995. Impact dynamics of composite beams. Composite Structures 32, 187–195.

Yigit, A.S., Christoforou, A.P., 2000. Control of low-velocity impact response in composite plates. Journal of Vibration and Control 6, 429–447.